CHEMISTRY OF MATERIALS

Article

pubs.acs.org/cm

Cubic Silica-Coated and Amine-Functionalized FeCo Nanoparticles with High Saturation Magnetization

Arati G. Kolhatkar,[†] Ivan Nekrashevich,[‡] Dmitri Litvinov,*[,‡,§,†] Richard C. Willson,*[,§] and T. Randall Lee*[,†]

[†]Department of Chemistry and Texas Center for Superconductivity, [‡]Department of Electrical and Computer Engineering, and [§]Department of Chemical and Biomolecular Engineering, University of Houston, 4800 Calhoun Road, Houston, Texas 77204, United States

ABSTRACT: By systematically varying the reaction parameters in a liquid-phase reduction reaction, large FeCo nanocubes with tunable body diagonal lengths of 175, 350, and 450 nm were synthesized. The nanocubes were initially stabilized with poly(vinyl pyrrolidone) (PVP) and then coated with a relatively thin layer of silica (~55 nm thick), which allowed them to retain their cubic shape. The magnetization curves showed that the PVP-stabilized nanocubes exhibited a high saturation magnetization of 167 ± 4 emu/g. The saturation magnetization, however, decreased upon coating with silica to 146 ± 13 emu/g for the particles with 350 and 450 nm FeCo cores and 48 ± 1 emu/g for the particles with 175 nm FeCo cores. The silica-coated FeCo nanocubes were then functionalized with 3-(aminopropyl)-trimethoxysilane (APTMS), and a layer of surface-bound nanoparticle was generated by exposing the resultant amine-functionalized nanocubes to self-assembled monolayers (SAMs) on gold terminated with carboxylic-acid groups.

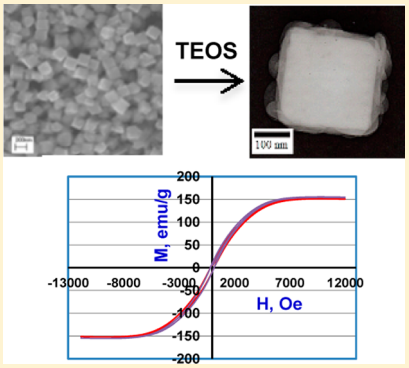

KEYWORDS: *cubic, silica-coated, FeCo, saturation magnetization, amine-functionalized, biosensor, nanoparticle, nanocube*

INTRODUCTION

The synthesis of spherical magnetic nanoparticles has been widely studied and continues to garner attention, because of their use in biosensing and biomedical applications.[1−3] For certain applications, however, geometries other than spherical are preferred (e.g., for applications involving magnetic-based biosensing devices, where a larger contact area of cubic nanoparticles can lead to more-robust binding to a sensor platform).[4] In addition, the increase in interfacial contacts and decrease in void fraction should lead to enhanced sensitivity and improved signal-to-noise ratios for cubic versus spherical magnetic nanoparticles.[5] Furthermore, although it is known that the properties of magnetic nanoparticles are strongly influenced by their size and shape,[6] magnetization data for some of the more common nanoparticle shapes are sorely lacking, particular for particles that have been coated with a thin layer of silica, which not only protects the magnetic cores from degradation,[7,8] but also permits their facile surface functionalization.[9]

In the work reported here, we systematically varied the reaction parameters in a liquid-phase reduction reaction to generate three distinct sizes of magnetic nanocubes, which we then coated with a relatively thin layer of silica. Previous reports of cubic FeCo described the synthesis of 68-nm FeCo nanocubes and nanocages with edge lengths of 500 nm.[10] Our modified recipe yielded FeCo nanocubes with body diagonals of 175 nm (edge length of ~100 nm), 350 nm (edge length of ~200 nm), and 450 nm (edge length of ~260 nm), respectively. Furthermore, we thoroughly characterized the magnetic properties (saturation magnetization and coercivity) of all these unique cubic particles, functionalized them with amine groups, and demonstrated the binding of the amine-functionalized nanocubes to a model sensor platform (i.e., a carboxylic-acid-terminated self-assembled monolayer (SAM) on gold).

For many sensing applications that rely on molecular recognition (e.g., ligand or antibody binding),[11,12] nanoparticles are coated with a robust, biocompatible, and readily modifiable protective layer. For many nanoparticles, silica is the coating of choice, because it meets these requirements.[13] We note that several studies have focused on embedding FeCo particles within a silica matrix,[14−16] and Zhang et al. have reported the coating of FeCo spheres using the Stöber process.[17,18] To our knowledge, however, the coating of cubic FeCo nanoparticles with silica *while retaining the cubic morphology after the coating process* has remained an elusive goal until now.

RESULTS AND DISCUSSION

Based on initial studies by Kodama et al., in which the relative concentrations of iron and cobalt precursors can be adjusted to control the shape of FeCo nanoparticles,[19] we prepared the PVP-stabilized FeCo nanocubes shown in Figure 1, together with their microscopy-derived size distributions. Importantly, the SEM and TEM images and the size distributions illustrate

Received: December 25, 2012
Revised: February 28, 2013
Published: March 1, 2013

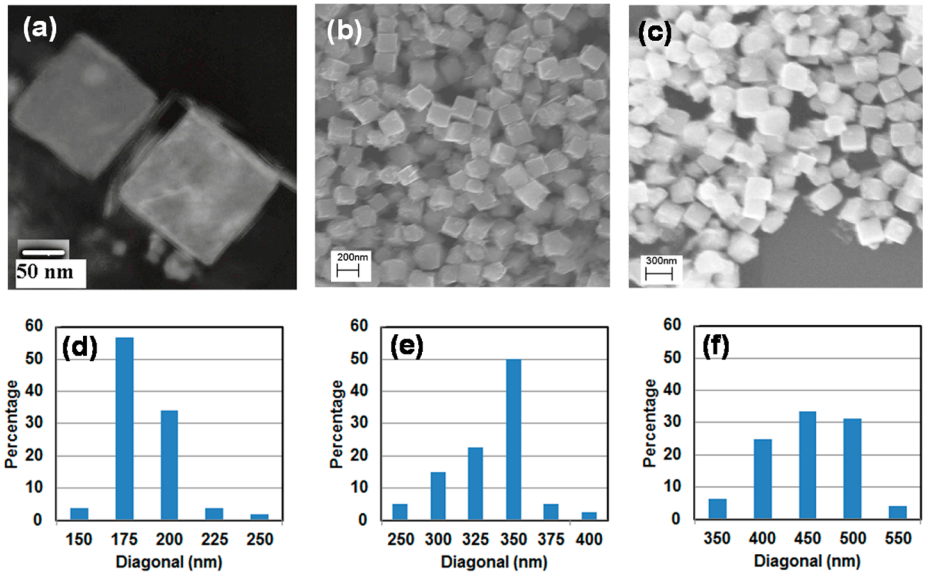

Figure 1. PVP-stabilized FeCo nanocubes: (a) TEM image of 175-nm particles and (d) the corresponding microscopy-derived size distribution; (b) SEM image of 50-nm particles and (e) the corresponding microscopy-derived size distribution; and (c) SEM image of 450-nm particles and (f) the corresponding microscopy-derived size distribution. Size distributions are based on 50−60 nanoparticles observed in an image. The sizes (given in nanometers) correspond to the mean cubic body diagonal.

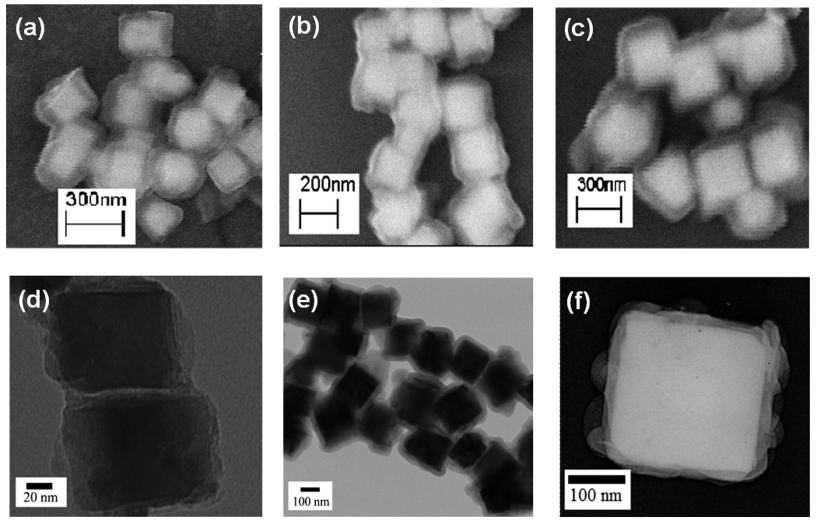

Figure 2. Top row: SEM images of silica-coated FeCo nanocubes (a) 175-nm FeCo with a silica layer 65 nm thick, (b) 350-nm FeCo with a silica layer 45 nm thick, and (c) 450-nm FeCo with a silica layer 45 nm thick. Panels (d), (e), and (f) in the bottom row show the corresponding TEM images.

both the cubic morphology of the nanoparticles and their monodisperse nature (except for the sample that contained the largest nanoparticles, which appear less uniform with regard to size and shape). Furthermore, as a complement to the previous studies,[19] the data in Figure 1 demonstrate our ability to tune the dimensions of the nanocubes from 175 nm to 450 nm simply by adjusting the reaction time. Notably, prior research that explored the synthesis of FeCo nanocubes and nanocages ranging in size from 68 to 110 nm were obtained at reactions times of 30 and 90 min, where the morphology changed from polyhedron to cubic as the time was increased from 2 min to 30−90 min.[10] For our purposes, a cubic morphology offers the advantage of increased interfacial binding to a two-dimensional (2D) substrate and enhanced sensitivity, compared to spherical nanoparticles; consequently, we focused on the synthesis of cubic FeCo nanoparticles and varied the reaction times beyond 30 min. Under these conditions, the nucleation rate is plausibly fast because hydrazine is a strong reducing agent for iron salts and cobalt salts; correspondingly, we observed a change in color from pink (Co(II) complex with hydrazine) to sea-green to black (nuclei) within less than 10 s after the addition of hydrazine (vide infra). Despite the fast nucleation, it should still be possible to sharpen the size distribution in the case of 450-nm FeCo nanoparticles by adjusting the temperature and the rate of agitation. In the present study, however, our further objective was the silica coating and amine functionalization; the moderately narrow distributions obtained are satisfactory for these purposes.

We used a modified Stöber process[9] to coat the FeCo nanocubes shown in Figure 2, where the thickness of the silica coating is ∼55 nm. Importantly, the SEM and TEM images confirm that the nanoparticles retain their cubic morphology

dx.doi.org/10.1021/cm304111z | *Chem. Mater.* 2013, 25, 1092−1097

after the coating process. Because of the high residual magnetization (discussed later), the nanocubes have a strong tendency to aggregate, creating challenges to the synthesis of silica-coated nanocubes that retain their cubic shape. Furthermore, although the nanoparticles might appear aggregated in the images in Figures 1 and 2, the surface of silica nanoparticles are negatively charged in ethanol (large negative zeta potentials),[20] which gives rise to good colloidal stability. However, because of the high saturation magnetization and coercivity of the FeCo core, it is impossible to keep the nanoparticles completely separated during imaging.

The silica-coated FeCo nanocubes were further characterized by XRD and EDX (Figure 3). The XRD pattern in Figure 3a of

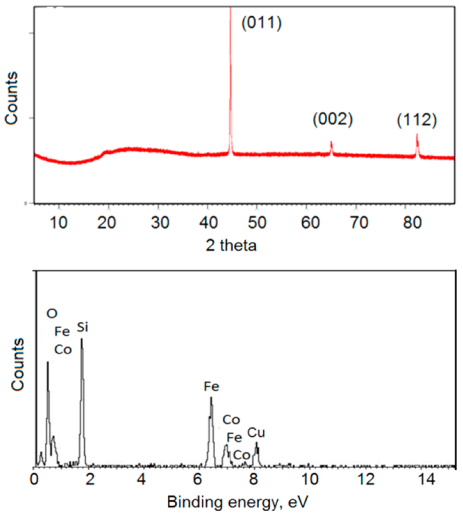

Figure 3. Silica-coated FeCo nanocubes (~450-nm FeCo core) analyzed via (a) X-ray diffraction (XRD) and (b) energy-dispersive X-ray analysis (EDX).

the 450-nm FeCo nanocubes matched the simple cubic structure of FeCo alloy, with peaks assigned to its (011), (002), and (112) reflections (JCPDS No. 49-1568).[12] Furthermore, the EDX data in Figure 3b show that composition of the FeCo nanocubes was $Fe_{72}Co_{28}$. Notably, the presence of Si and O peaks confirm that the nanocubes were coated with silica, and the composition of silica was found to be $SiO_{1.4}$.

The nanoparticles were then functionalized with amine groups, which gives rise to large positive zeta potentials in ethanol and thus good colloidal stability.[20] The amine functionalization was confirmed using X-ray photoelectron spectroscopy (XPS), where the spectra in Figure 4 show a clear peak at 400 eV, indicating the presence of nitrogen. In the same figure, comparison is made to the bare silica-coated nanocube precursors, where the absence of nitrogen is consistent with no amine functionalization. The ratio of the atomic percentages of oxygen (binding energy 533 eV) and silicon (binding energy 103 eV) was 2.3 ± 0.1 to 1, which is consistent with the expected stoichiometry.

We then explored the binding of the amine-functionalized nanoparticles to a model sensor platform—a carboxylic acid-functionalized SAM substrate, where the SAM was generated from the adsorption of 16-mercaptohexadecanoic acid on gold.[21] A typical SAM with a S–S spacing of 5 Å for the adsorbate headgroups will correspond to ~6×10^5 molecules of 16-mercaptohexadecanoic acid on the 400 nm × 400 nm sensor. This degree of coverage will ensure that any

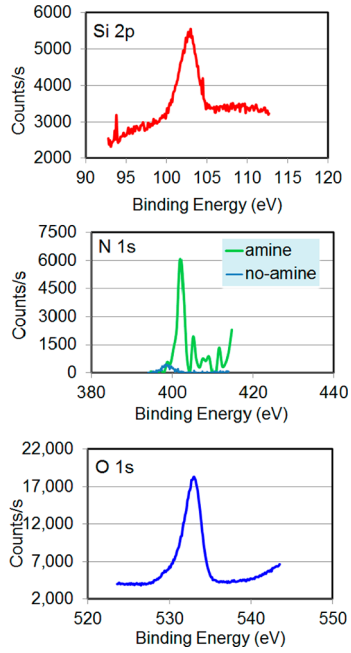

Figure 4. X-ray photoelectron spectroscopy (XPS) data for the amino-functionalized silica-coated FeCo nanocubes with comparison to the precursor nanocubes for the XPS spectra collected in the N 1s region.

approaching amine-functionalized nanocubes will be attracted to the carboxylic acid-terminated surface and become electrostatically bound. To produce an adsorbed nanocube array, the SAM-coated wafer was placed in a suspension of amino-functionalized FeCo nanocubes in ethanol for 1 h at room temperature (rt), and the wafer was then rigorously and repeatedly washed with ethanol and water to remove any weakly bound nanoparticles from the SAM surface. The SEM image in Figure 5 demonstrates the binding of these nanocubes

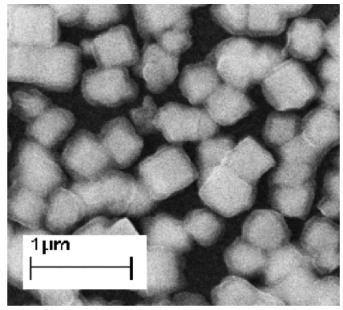

Figure 5. SEM image of 450-nm amino-functionalized FeCo nanocubes electrostatically bound to a carboxylic acid-terminated gold-coated wafer. Any weakly bound nanoparticles were removed by multiple washings with ethanol and water.

to the SAM-coated gold surface, and it also offers experimental support (albeit indirect) for the effectiveness of the amine functionalization. Importantly, the strongly bound layer of nanoparticles provides a rudimentary demonstration of the sensing platform, which is one of the ultimate goals of our research.[22−24]

With regard to biosensing applications, our targeted magnetoresistance-based sensor platform consists of consecutive layers of Co/Cu/Co that are coated with a thin layer of alumina or silica and then functionalized with a molecular

dx.doi.org/10.1021/cm304111z | Chem. Mater. 2013, 25, 1092−1097

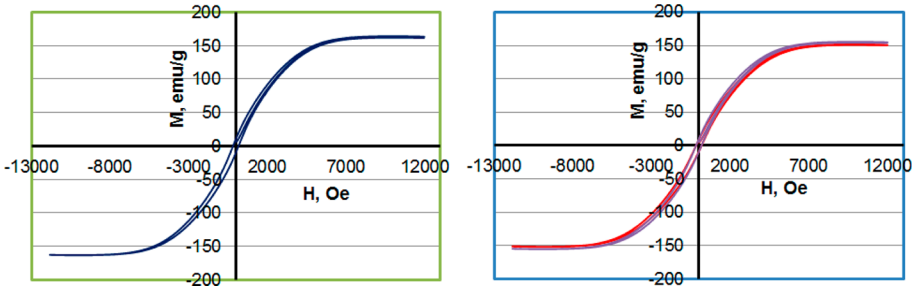

Figure 6. Magnetization curves for 450-nm FeCo nanocubes (a) as PVP-stabilized particles and (b) as silica-coated nanoparticles, from two independent syntheses.

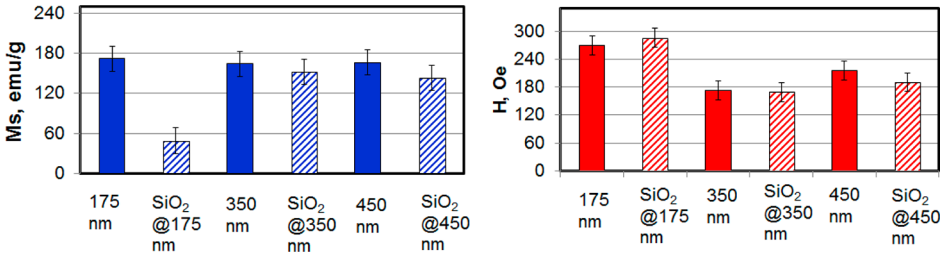

Figure 7. Bar graphs showing the average saturation magnetization and average coercivity for 175-, 350-, and 450-nm PVP-stabilized FeCo nanocubes.

recognition element. Magnetic nanoparticles decorated with a complementary target biomarker will bind to the sensor by direct or sandwich assays, and these magnetic nanoparticles will be detected via a corresponding change in magnetoresistance.[25] We designed and built this sensing platform with the capacity to detect a single 100-nm spherical Fe_3O_4 nanoparticle having 60−80 emu/g, which corresponds to a sensitivity of $\sim 10^{-13}$ emu. Our cubic FeCo nanoparticles with body diagonals of 175, 350, and 450 nm have a markedly higher saturation magnetization (vide infra) and thus can be readily detected using this sensing platform. Notably, based on the dimensions of our sensor and FeCo nanocubes, we can estimate a maximum binding of 16 (for 175 nm), 4 (for 350 nm), and 2 (for 450 nm) nanoparticles during a given measurement.

The magnetic properties of the PVP-stabilized and silica-coated FeCo nanocubes were characterized by vibrating sample magnetometry (VSM). Figure 6 shows the obtained magnetization curves, which indicate a saturation magnetization of 166 emu/g and a coercivity (H) of 215 Oe for the 450-nm PVP-stabilized FeCo nanocubes. Unsurprisingly, for both sets of the 450-nm silica-coated FeCo nanoparticles, the saturation magnetization on a per-gram basis is noticeably lower (as expected due to the mass of the nonmagnetic silica coating). Furthermore, as indicated by the bar graphs in Figure 7, the average saturation magnetization for all sizes of the PVP-stabilized FeCo nanocubes (having composition $Fe_{72}Co_{28}$ as noted above) was 168 ± 4 emu/g, which is similar in magnitude to the saturation magnetization of bulk $Fe_{70}Co_{30}$ (240 emu/g)[26] and bulk $Fe_{65}Co_{35}$ (245 emu/g).[27]

We note that Lu et al.[27] studied the size-dependent saturation magnetization of γ-Fe_2O_3, $CoFe_2O_4$, and $MnFe_2O_4$ nanoparticles and found that, beyond a certain size unique for each material, the ratio of saturation magnetization of the sample to that of the bulk value ($M_s/M_{s,bulk}$) is constant. In the case of our FeCo nanocubes, the $M_s/M_{s,bulk}$ ratio was also found to be constant for the three sizes examined.

In contrast to the PVP-stabilized FeCo nanocubes, the saturation magnetization of the 175-nm silica-coated FeCo nanocubes was 48 ± 1 emu/g for 175 nm, and that for both the 350- and 450-nm silica-coated FeCo nanocubes was 146 ± 13 emu/g. The decrease in magnetization on a per-gram basis is due to the increase in the mass of the nonmagnetic component (silica). Since the mass, for example, of each 175-nm nanocube increased from ~8 fg to ~33 fg upon coating with silica, the observed ~4-fold decrease in the M_s value (172 emu/g vs 48 emu/g) is attributed to the ~4-fold increase in the mass of the nanoparticles. An analogous but less pronounced correlation can be drawn with the magnetization data for the 350- and 450-nm FeCo nanocubes.

Based on the magnetization curves obtained and the hysteresis trends observed in Figure 6, the FeCo nanocubes prepared here are not superparamagnetic. Nevertheless, they can be readily manipulated by an external magnetic field. Furthermore, the observed strong saturation magnetization, coupled with their facile functionalization and subsequent binding to a model sensor platform, offers evidence that these silica-coated FeCo nanocubes warrant further investigation in magnetic biosensing applications.

EXPERIMENTAL SECTION

FeCo Synthesis. We prepared FeCo nanocubes using a modification of a known liquid-phase reduction reaction.[10] The chemicals used in the synthesis were analytical grade and used without purification. Millipore water (resistivity of >18 MΩ cm) was used in the synthesis and washing steps. The wet chemical precipitation/synthesis involved reduction of aqueous Fe^{2+} and Co^{2+} with hydrazine and was performed in the presence of poly(ethylene glycol) and cyclohexane. Ferrous sulfate (0.7 g $FeSO_4{\cdot}7H_2O$), cobalt chloride (0.175 g $CoCl_2{\cdot}4H_2O$), poly(ethylene glycol) (8 mL PEG-440 g/mol), and cyclohexane (0.8 mL) were dissolved in 50 mL of water. This mixture was sonicated for 1.5 h at rt and then heated to 78 °C, using an oil bath. A solution of hydrazine (20 mL of NH_2NH_2) and sodium hydroxide (2.5 g of NaOH) was added to the heated mixture. After 30 min, a black precipitate was obtained, which was washed three times with water and then once with toluene and acetone before drying

dx.doi.org/10.1021/cm304111z | Chem. Mater. 2013, 25, 1092−1097

under vacuum at rt. The molar ratio of Fe^{2+}/Co^{2+} was held constant in all of the nanoparticle syntheses, but the reaction time was varied to obtain cubes of varying sizes; specifically, reaction times of 30, 40, and 45 min afforded FeCo nanocubes with body diagonals of 175 nm (edge length ≈ 100 nm), 350 nm (edge length ≈ 200 nm), and 450 nm (edge length ≈ 260 nm), respectively. The length dimension for nanocubes described refers to the body diagonal. The length of the body diagonal was calculated using the following geometric relationship: body diagonal (in nanometers) = $\sqrt{3}$(cube side, in nanometers).

Silica Coating. The FeCo nanocubes were stabilized with poly(vinyl pyrrolidone) (PVP, MW 10 000 g/mol) prior to coating them with silica. An aliquot of black FeCo powder (0.045 g) was suspended in 0.2−0.4 mL of a 1% PVP solution in 20 mL of ethanol, sonicated for 3 h at 69 °C, and then mechanically agitated at the same temperature overnight. The PVP-stabilized FeCo nanocubes were washed multiple times with water and ethanol, centrifuged, and dried in a vacuum oven overnight. We used a modified version of the Stöber process[9] to coat the PVP-functionalized FeCo nanocubes with silica. Approximately 10−25 mg of PVP-stabilized FeCo nanocubes were dispersed in 20 mL of ethanol and 2.2 mL of water, and the mixture was sonicated for 30 min. To this mixture, 1.3 mL of 30% ammonium hydroxide (NH_4OH) and 0.1 mL tetraethyl orthosilicate (TEOS) was added to initiate the reaction under mechanical agitation, which was continued for 4−5 h. The sample was separated using a bar magnet and washed multiple times with ethanol and water.

Amine Functionalization. We used (3-aminopropyl)-trimethoxysilane (APTMS) to decorate the surface of the silica-coated nanocubes with amino groups. To a 20-mL suspension of silica-coated nanoparticles in ethanol, we added 0.2 mL APTMS and 0.1 mL of water with mechanical agitation overnight.

Characterization. These nanocubes and selected samples of their progeny were characterized using transmission electron microscopy (TEM) (JEOL, Model JEOL-2000 FX, operating at 200 kV with attached energy-dispersive X-ray spectroscopy (EDX)), scanning electron microscopy (SEM) (LEO, Model LEO-1525 operating at 15 kV), X-ray photon spectroscopy (XPS) (Physical Electronics, Model PHI 5700 XPS with an Al Kα X-ray source), vibrating sample magnetometry (VSM) (LakeShore, Model VSM 7300 Series with a LakeShore Model 735 Controller and LakeShore Model 450 Gmeter Software, Version 3.8.0), and X-ray diffraction (XRD) (Siemens, Model D5000 X-ray diffractometer). For the TEM analyses, the nanoparticles were deposited on a 300-mesh holey carbon-coated copper grid and allowed to dry; for the SEM analyses, the nanoparticles were deposited on a silicon wafer and allowed to dry. Each of the size histograms was generated via the analysis of 50−60 particles. The magnetic properties (saturation magnetization, residual magnetization, and coercivity) of a known mass of sample were measured using VSM. For additional compositional and structural confirmation, we used EDX and XRD to characterize the nanocubes. For the latter studies, a concentrated sample of FeCo in ethanol was deposited on a piranha-cleaned glass slide, and XRD was carried out using Cu Kα radiation (λ = 1.540562 Å) in the 2θ range of 0°−90°. We also used XPS to confirm the presence of the silica coating on the FeCo nanocubes and demonstrate the subsequent amino functionalization with APTMS; for these studies, the nanocubes were dispersed in ethanol, deposited on a gold-coated silicon wafer, and allowed to dry.

AUTHOR INFORMATION

Corresponding Author

*E-mail addresses: litvinov@uh.edu (D.L.), willson@uh.edu (R.D.W.), trlee@uh.edu (T.R.L.).

Author Contributions

All authors have given approval to the final version of the manuscript.

Notes

The authors declare no competing financial interest.

ACKNOWLEDGMENTS

We thank the following funding sources for generously supporting this research: the National Institutes of Health (NIH) (No. ARRA-1RC1RR028465-01), the National Science Foundation (NSF) (No. ECCS-0926027), the Robert A. Welch Foundation (No. E-1320 to T.R.L. and No. E-1264 to R.C.W.). We also acknowledge financial support from the Texas Center for Superconductivity at the University of Houston. We also thank Dr. Sang Ho Lee for providing the XRD data, and Drs. Pawilai Chinwangso, Boris Makarenko, and Irene Rusakova for helpful advice and technical assistance.

REFERENCES

(1) Tran, N.; Webster, T. *J. Mater. Chem.* **2010**, *20*, 8760−8767.
(2) McBain, S. C.; Humphrey, H. P. Y.; Dobson, J. *Int. J. Nanomed.* **2008**, *3*, 169−180.
(3) Roca, A. G.; Costo, R.; Rebolledo, A. F.; Veintemillas-Verdaguer, S.; Tartaj, P.; Gonzalez-Carreno, T.; Morales, M. P.; Serna, C. J. *J. Phys. D: Appl. Phys.* **2009**, *42*, 1−12.
(4) Sau, T.; Rogach, A. L. *Adv. Mater.* **2010**, *22*, 1781−1804.
(5) Dovgolevsky, E.; Haick, H. *Small* **2008**, *2*, 2059−2066.
(6) Treguer-Delapierre, M.; Majimel, J.; Mornet, S.; Duguet, E.; Ravaine, S. *Gold Bull.* **2008**, *41*, 195−207.
(7) Guerrero-Martinez, A.; Perez-Juste, J.; Liz-Marzan, L. M. *Adv. Mater.* **2010**, *22*, 1182−1195.
(8) Selvan, S. T. *Biointerphases* **2010**, *5*, FA10−FA15.
(9) Weichold, O.; Tigges, B.; Bertmer, M.; Moller, M. *J. Colloid Interface Sci.* **2008**, *324*, 105−109.
(10) Wei, X.; Zhu, G.; Liu, Y.; Ni, Y.; Song, Y.; Xu, Z. *Chem. Mater.* **2008**, *20*, 6248−6253.
(11) Baselt, D. R.; Lee, G. U.; Natesan, M.; Metzger, S. T.; Sheehan, P. E.; Colton, R. J. *Biosens. Bioelectron.* **1998**, *13*, 731−739.
(12) Koh, I.; Josephson, L. *Sensors* **2009**, 8130−8145.
(13) Guerrero-Martinez, A.; Perez-Juste, J.; Liz-Marzan, L. M. *Adv. Mater.* **2010**, *22*, 1182−1195.
(14) Thirumal, E.; Prabhu, D.; Chattopadhyay, K.; Ravichandran, V. *Phys. Status Solidi A* **2010**, *207*, 2505−2510.
(15) Carta, D.; Casula, M. F.; Bullita, S.; Falqui, A.; Corrias, A. *J. Nanopart. Res.* **2011**, *13*, 3489−3501.
(16) Falqui, A.; Corrias, A.; Gass, M.; Mountjoy, G. *Microsc. Microanal.* **2009**, *15*, 114−124.
(17) Zhang, K.; Holloway, T.; Bahoura, M.; Pradhan, A.; Prabakaran, R.; Pradhan, J.; Smith, S.; Hall, J.; Ramesh, G.; Sahu, D.; Huang, J.-L. *Proc. SPIE* **2009**, *7291*, 729104-1−729104-10.
(18) Harris, M. T.; Brunson, R. R.; Bryers, C. H. *J. Non-Cryst. Solids* **1990**, *121*, 397−403.
(19) Kodama, D.; Shinoda, K.; Sato, K.; Konno, Y.; Joseyphus, R. J.; Motomiya, K.; Takahashi, H.; Matsumoto, T.; Sato, Y.; Tohji, K.; Jeyadevan, B. *Adv. Mater.* **2006**, *18*, 3154−3159.
(20) Graf, C.; Qi Gao, Q.; Schutz, I.; Noufele, C.; Ruan, W.; Posselt, U.; Korotianskiy, E.; Nordmeyer, D.; Fiorenza, R.; Hadam, S.; Vogt, A.; Lademann, J.; Haucke, V.; Ruhl, E. *Langmuir* **2012**, *28*, 7598−7613.
(21) Chingwangso, P.; Jamison, A. C.; Lee, T. R. *Acc. Chem. Res.* **2011**, *44*, 511−519.
(22) Gaster, R. S.; Xu, L.; Han, S.-J.; Wilson, R. J.; Hall, D. A.; Osterfeld, S. J.; Yu, H.; Wang, S. X. *Nat. Nanotechnol.* **2011**, *6*, 314−320.
(23) Dittmer, W. U.; Kievet, P.; Prins, M. W. J.; Vissers, J. L. M.; Mersch, M. E. C.; Martens, M. F. W. C. J. *J. Immunol. Methods* **2008**, *338*, 40−46.
(24) Osterberg, F. W.; Dalslet, B. T.; Damsgaard, C. D.; Freitas, S. C.; Freitas, P. P.; Hansen, M. F. *IEEE Sens. J.* **2009**, *9*, 682−688.
(25) Litvinov, D.; Willson, R. U.S. Patent Application No. 20100188075, 2010.
(26) Wei, X.; Zhu, G.; Liu, Y.; Ni, Y.; Song, Y.; Xu, Z. *Chem. Mater.* **2008**, *20*, 6248−6253.

(27) Lu, H. M.; Zheng, W. T.; Jiang, Q. *J. Phys. D: Appl. Phys.* **2007**, *40*, 320−325.